Multimodal analyses reveal genes driving electrophysiological maturation of neurons in the primate prefrontal cortex

Yu Gao[1,9], Qiping Dong[1,9], Kalpana Hanthanan Arachchilage[1,9], Ryan D. Risgaard[1], Moosa Syed[1], Jie Sheng[1], Danielle K. Schmidt[1], Ting Jin[1], Shuang Liu[1], Sara Knaack[1], Dan Doherty[2], Ian Glass[2], Jon E. Levine[3,4], Daifeng Wang[1,5,6]*, Qiang Chang[1,7,8]*, Xinyu Zhao[1,3]*, André M. M. Sousa[1,3]*

[1]Waisman Center, University of Wisconsin-Madison; Madison, WI, USA

[2]Department of Pediatrics, University of Washington School of Medicine; Seattle, WA, USA

[3]Department of Neuroscience, University of Wisconsin-Madison; Madison, WI, USA

[4]Wisconsin National Primate Research Center, University of Wisconsin-Madison; Madison, WI 53705

[5]Department of Biostatistics and Medical Informatics, University of Wisconsin-Madison; Madison, WI, USA

[6]Department of Computer Sciences, University of Wisconsin-Madison; Madison, WI, USA

[7]Department of Medical Genetics, University of Wisconsin-Madison; Madison, WI, USA

[8]Department of Neurology, University of Wisconsin-Madison; Madison, WI, USA

[9] These authors contributed equally to this work.

*Correspondence: André M. M. Sousa (andre.sousa@wisc.edu), Xinyu Zhao (xinyu.zhao@wisc.edu), Qiang Chang (qchang@waisman.wisc.edu), Daifeng Wang (daifeng.wang@wisc.edu)

SUMMARY

The prefrontal cortex (PFC) is critical for myriad high-cognitive functions and is associated with several neuropsychiatric disorders. Here, using Patch-seq and single-nucleus multiomic analyses, we identified genes and regulatory networks governing the maturation of distinct neuronal populations in the PFC of rhesus macaque. We discovered that specific electrophysiological properties exhibited distinct maturational kinetics and identified key genes underlying these properties. We unveiled that RAPGEF4 is important for the maturation of resting membrane potential and inward sodium current in both macaque and human. We demonstrated that knockdown of *CHD8*, a high-confidence autism risk gene, in human and macaque organotypic slices led to impaired maturation, via downregulation of key genes, including *RAPGEF4*. Restoring the expression of *RAPGEF4* rescued the proper electrophysiological maturation of CHD8-deficient neurons. Our study revealed regulators of neuronal maturation during a critical period of PFC development in primates and implicated such regulators in molecular processes underlying autism.

INTRODUCTION

The dorsolateral prefrontal cortex (dlPFC), a neocortical area highly derived in primates[1-3], is required for higher-order brain functions, including executive functions such as working memory, planning, and decision-making[3-5]. These functions are significantly impaired in brain disorders, including autism spectrum disorders (ASD), schizophrenia, obsessive-compulsive disorder, and neurodegenerative disorders[6-8]. Much of our knowledge on PFC development is largely extrapolated from rodent studies. Although rodents possess a PFC that is homologous to a small portion of the primate PFC, they lack the granular dlPFC[1]. Several comparative studies have

54 identified gene expression signatures that are unique to the PFC of humans and non-human
55 primates (NHP)[3,9-12]. Therefore, it is essential to understand the mechanisms regulating dlPFC
56 development in primates.

57 The cells that compose the primate dlPFC, especially excitatory and inhibitory neurons,
58 undergo extensive and dynamic maturation throughout midfetal and late-fetal development, during
59 which critical neurodevelopmental events, such as circuit assembly and electrophysiological
60 maturation of neurons occur[13]. Midfetal and late-fetal development are a convergent period of
61 expression for many ASD genes[14,15], yet the functions of these ASD genes during this period of
62 development remains unclear. Furthermore, although we have a robust knowledge of the molecular
63 and cellular mechanisms that govern cell fate specification during cortical development[16-22], and
64 of the transcriptomic and electrophysiological properties of mature neurons in the adult
65 neocortex[23-27], our understanding of the gene networks that regulate the early stages of neuronal
66 maturation, especially electrophysiological maturation, remains elusive. Therefore, a multimodal
67 investigation of primate dlPFC neurons that combines electrophysiological and functional
68 genomic analyses during critical periods for neuronal maturation is essential to understand the
69 mechanisms driving neuronal maturation.

70 Here, to uncover the molecular mechanisms that regulate the maturation of dlPFC neurons,
71 we first generated single-nucleus multiomic (snMultiomic) data and performed integrated analyses
72 of the dlPFC from rhesus macaques (*Macaca mulatta)*, ranging from midfetal to late-fetal periods.
73 We then performed Patch-seq on acute dlPFC slices from 16 macaques, including the same
74 specimens profiled for snMultiome. This approach allowed us to integrate our electrophysiological
75 analyses with gene expression profiles to identify the genes that are important for the maturation
76 of specific electrophysiological features. Furthermore, we have evaluated the function of select

77 genes – *RAPGEF4* and *CHD8* – and demonstrated that a loss of function of these genes affects the
78 morphological and electrophysiological maturation of cortical neurons in organotypic slices of
79 macaque and human. Finally, Patch-seq analysis of brain slices with *CHD8* knockdown identified
80 RAPGEF4 as a key mediator for CHD8 regulation of electrophysiological maturation of human
81 cortical neurons.
82

83 **RESULTS**

84 **Cell type-specific transcriptomic changes underlying the maturation of rhesus macaque**
85 **dlPFC cells during midfetal and late-fetal development**

86 We performed snMultiomic analyses on 9 rhesus macaque dlPFC samples across eight prenatal
87 ages: postconceptional day (PCD) 85, PCD95, PCD100, PCD105, PCD110, PCD125, PCD145,
88 and two PCD155 (**Figures 1A-1B; Table S1**). After implementing stringent quality control
89 measures, we retained 76,855 nuclei for further analyses (**Figures S1; Tables S1-S2**). After
90 removing batch effects, we used unsupervised clustering to group nuclei into transcriptomically
91 defined groups (**Figures S1B-S1C**). Using this strategy, together with cell type-specific marker
92 genes[16,23,28], we defined 9 major cell classes that included glutamatergic excitatory neurons (ExN),
93 GABAergic inhibitory neurons (InN), glial progenitor cells (GPC), astrocytes, oligodendrocyte
94 precursor cells (OPC), oligodendrocytes, microglia, vascular leptomeningeal cells (VLMC), and
95 endothelial cells (**Figure S2A**). We re-clustered the ExN and InN nuclei to identify their subclasses
96 based on the layer (L) and projection identity (intratelencephalic [IT], extratelencephalic [ET],
97 near-projecting [NP], corticothalamic [CT], and L6B) for ExN, and the developmental origin
98 (medial ganglionic eminence [MGE], caudal ganglionic eminence [CGE], or dorsal lateral
99 ganglionic eminence [dLGE]) for InN (**Figures 1C and S2B-S2C**). Interestingly, one small

100 population of IT neurons exhibited molecular features of both ExN L2-3 IT and ExN L3-5 IT,
101 indicating that this small population of neurons is yet to be fully specified; we classified this
102 population as ExN L2-3 IT/L3-5 IT. At the lowest hierarchical level of cell type classification, we
103 transcriptomically defined 85 cell subtypes (**Figure S2E; Table S3**). By integrating our dataset
104 with two published snRNA-seq datasets that analyzed early fetal[28] and adult[23] macaque dlPFC, we
105 observed that our data bridges the embryonic/early fetal cell types with the adult cell types,
106 facilitating the tracing of the developmental origins of distinct adult cell subtypes (**Figures 1E-**
107 **1G**).

108 As expected, we observed an increasing number of glial cells, including astrocytes, OPCs,
109 and oligodendrocytes throughout late-fetal development (**Figure 1D**), a period characterized by
110 minimal cortical neurogenesis and robust gliogenesis[29]. Within the excitatory neurons, we
111 observed that IT neurons were more abundant than any other subclass, as previously described in
112 the adult dlPFC[23]. The selective expansion of IT neurons in the primate lineage, especially of
113 upper-layer (L2-3) neurons[23] and their functional relevance in the cortico-cortical circuits that
114 govern some of the unique cognitive and behavioral abilities of primates[30], led us to focus our
115 analysis on the maturational profiles of these IT neuronal populations: ExN L2-3 IT and ExN L3-
116 5 IT (**Figures 2A-2D**). We performed differential gene expression analysis along the
117 developmental trajectory (i.e., pseudotime) to identify genes that display dynamic, highly variable
118 changes during neuronal maturation. Among the top 100 genes (**Table S4**), we observed genes
119 that exhibit cell type-specific correlation with maturation (**Figures 2C-2D**), including *MEIS2*, a
120 transcriptional regulator that is induced by retinoic acid and is important for the arealization of the
121 prefrontal cortex[10], in L2-3 IT, and *FOXP2*, a gene encoding a transcription factor that has recently

been shown to have primate-specific expression in L3-5 IT excitatory neurons[23]. Disruptions in these genes have been linked to neuropsychiatric disorders[31,32].

Together, our analyses uncovered the transcriptional landscape of primate midfetal and late-fetal PFC development, highlighting differences between distinct excitatory neuronal populations throughout maturation.

Chromatin accessibility signatures and gene regulatory networks of macaque midfetal and late-fetal dlPFC cells

The simultaneous profiling of gene expression and chromatin accessibility in the same cells allows linking putative regulatory elements to genes, thus providing insights into cell-type gene regulatory mechanisms in the developing primate brain. After filtering out low-quality nuclei and implementing other stringent quality control steps, snATAC-seq data from 64,941 nuclei were retained for downstream analyses (**Figure S1D**). We observed that the clustering of cells based on accessible chromatin was similar to the clustering utilizing gene expression data (**Figures S1E-S1H**), showing the congruence between the two datasets (**Figure 3A**). However, the snATAC-seq data revealed more pronounced differences in the maturation states of cells within each cell subclass, especially for IT excitatory neurons (**Figure S1E**). To gain a better understanding of the association of regulatory elements and their target genes during neuronal maturation, we estimated peak-to-gene links, which identify co-activity between genes and their nearby accessible chromatin regions, for the excitatory and inhibitory neurons (**Figure S3A**), thus providing a list of potential regulatory elements for each gene (**Table S5**). We found that peak-gene combinations were hierarchically divided into three distinct categories: a cluster specific to excitatory neurons during early midfetal development, a cluster specific to excitatory neurons during late-fetal

145 development, and a cluster specific to inhibitory neurons during late-fetal development. Functional
146 enrichment analysis of each group revealed that the clusters specific to late-fetal development were
147 enriched for terms related to calcium signaling and dendritic development in excitatory neurons,
148 and synaptic processes in inhibitory neurons, whereas the early-midfetal development cluster was
149 enriched for transcriptional regulation terms (**Figures S3C-S3E; Table S5**).

150 Next, since gene expression is regulated by gene regulatory networks (GRNs)[33] and
151 expression of genes associated with ASD converge in excitatory neurons during these
152 developmental stages in ExN L2-3 IT and ExN L3-5 IT cell subclasses[14,15], we inferred cell-type
153 gene regulatory networks (GRNs) for these two cell subclasses using transcriptomic and
154 epigenomic data together with transcription factor (TF) motif binding sites (**Methods**). These cell-
155 type GRNs link regulatory elements with TF binding sites to target genes. We particularly focused
156 on analyzing the subnetworks regulating the genes identified in our developmental maturation
157 trajectory analysis (**Table S4**) and found nine major TFs regulating the driver genes of the two cell
158 subclasses. Among these nine TFs, we identified MEIS2 as a key regulator for ExN L2-3 IT,
159 FOXP2 as a hub TF for ExN L3-5 IT, and MEF2C as an important TF for both ExN subclasses
160 (**Figure 3B**).

161 Since upper-layer (L2-3) neurons exhibit selective expansion in the primate lineage[23] and
162 their roles in the cortico-cortical circuits that are important for the unique cognitive and behavioral
163 abilities of primates[30], we investigated putative regulatory elements that underlie the
164 transcriptomic differences between ExN L2-3 IT and ExN L3-5 IT. We calculated differential
165 accessibility and overrepresented motifs between these neuronal populations throughout midfetal
166 and late-fetal development. Using this strategy, we identified the MEIS2 motif MA0774.1 as one
167 of the overrepresented motifs in the ExN L2-3 IT subclass (**Table S6**). Furthermore, we found that

168 ExN L2-3 IT has both higher *MEIS2* gene expression and a higher MEIS2 motif activity score
169 when compared to ExN L3-5 IT (**Figure 3C**). Because MEIS2 is a transcription factor enriched in
170 upper-layer neurons in primates[10,23] and is implicated in neuropsychiatric disorders[32], we
171 calculated MEIS2 transcription factor footprints across the whole genome in the two cell
172 subclasses and found that, throughout the analyzed developmental periods, ExN L2-3 IT had a
173 higher footprint enrichment than ExN L3-5 IT, with the highest enrichment in ExN L2-3 IT during
174 midfetal development (PCD105-110) and the lowest footprint enrichment in ExN L3-5 IT during
175 late fetal development (PCD155), indicating the selective involvement of MEIS2 in the regulation
176 of target genes in ExN L2-3 IT (**Figure 3C**). Indeed, quantitative immunofluorescence showed
177 that there were significantly fewer MEIS2-expressing cells in L3-5, identified by the expression
178 of *RORB* (**Figure S3B**), compared to L2-3 of dlPFC at PCD155 (**Figure 3D**).

179 One of the genes potentially regulated by MEIS2 in IT excitatory neurons is the *Nuclear*
180 *factor I/A* (*NFIA*), which has been shown to be regulated by MEIS2 in retinal progenitor cells[34]
181 and is linked to callosal hypoplasia, likely reflecting malformations of upper-layer excitatory
182 neurons[35]. By analyzing the distribution of accessible chromatin peaks in the vicinity of *NFIA*
183 across the two neuronal subclasses and developmental periods, we identified 5 active MEIS2
184 binding sites within 200kb upstream of the *NFIA* transcription start site (**Figure 3E**). We also
185 found three peak-to-gene links (peaks that show higher co-activity with *NFIA* gene expression),
186 with one of the links containing two predicted MEIS2 binding motifs (chr1-163553896-
187 163555161) approximately 181kb upstream of the *NFIA* transcription starting site, suggesting that
188 it may be a potential regulatory element for *NFIA*. To validate this finding, we conducted a dual
189 luciferase assay to assess the activity of the genomic sequence containing the two MEIS2 motifs.
190 Overexpression of MEIS2 resulted in a significant increase in transcription activity driven by the

genomic sequence. Furthermore, when we introduced mutations into two potential MEIS2 binding motifs, one of these mutations significantly reduced the activity of the genomic sequence (**Figure 3F**). Taken together, our analyses have unveiled key regulators, such as MEIS2, and gene regulatory networks governing the maturation of distinct IT neuronal populations during midfetal and late-fetal primate brain development.

Patch-seq of midfetal and late-fetal macaque dlPFC cells identified transcriptomic signatures defining electrophysiological maturation

The midfetal and late-fetal periods are critical stages in cortical development, marked by notable alterations in neuronal morphology, electrophysiology, and gene expression[13]. Although all the analyzed neurons displayed a relatively immature morphology, PCD155 neurons exhibited significantly greater complexity, with greater total dendritic length, increased branching points, and more endings when compared to neurons from PCD100 brains (**Figures S4B-S4F**). To gain a comprehensive understanding of the molecular mechanisms that drive neuronal maturation, we employed Patch-seq, which allows for sequential electrophysiological and transcriptomic analyses of the same cell[36], in 16 rhesus macaques ranging from PCD85 to PCD155 (**Figures 4A and S4; Table S1**). We used our snRNA-seq data (**Figure 2**) as the reference dataset to infer cell types by mapping the 256 cells profiled by Patch-seq onto the reference UMAP (**Figures 4B and S4I; Table S7**). Approximately 72% of all cells were identified as neurons based on their transcriptomic signature, which included 111 IT neurons (**Table S7**). Our evaluation of the electrophysiological features of three major IT subtypes (L2-3, L3-5, and L6) across different ages revealed that these IT neurons exhibited similar electrophysiological features (**Figures S4J-S4N**) during this developmental window. Therefore, we combined all IT neuron types for downstream analysis.

214 We employed a pseudotime trajectory analysis to infer a maturation trajectory by
215 integrating differentially expressed genes across age groups in all identified IT neurons (**Methods**).
216 Our analysis revealed a trajectory characterized by the progressive maturation of IT neurons from
217 earlier to later developmental periods (**Figure 4C**). We observed that the proportion of IT neurons
218 exhibiting action potentials (APs) across six age groups (PCD85-90, PCD95-100, PCD105-110,
219 PCD125, PCD145, and PCD155) gradually increased from 0% in the PCD85-90 group to 95% in
220 PCD155, providing strong evidence for electrophysiological maturation (**Figure S4O**). We then
221 assessed neuronal maturation through the lens of the following features that offer unique
222 perspectives on maturation: membrane capacitance (C_m), input resistance (R_{in}), resting membrane
223 potential (RMP), and inward sodium current (I_{Na}). Our analysis revealed that, during early midfetal
224 development (from PCD85 to PCD100), none of the electrophysiological features showed
225 significant change (**Figure 4**). We observed a significant increase in C_m from PCD100 to PCD105,
226 after which the values remained stable (**Figure 4**). This increase in C_m potentially reflects the
227 enlargement of the cell body and more complex cellular structures during the maturation of
228 neurons. In contrast, there was a gradual decline in the averaged value of R_{in} after PCD125 (**Figure**
229 **4F**). This effect may be attributed to an increase in the number of ion channels in the neuronal
230 membrane. Moreover, the morphological changes that occur in dendrites (**Figures S4B-S4F**) and
231 spines during maturation may contribute to alterations in signal processing and integration, further
232 enhancing neuronal function. We also observed a conspicuous pattern of increasingly negative
233 RMP from PCD100 to PCD155 (**Figure 4G**), which reflects the developmental maturation in the
234 ion channel composition of these neurons, allowing for improved electrical signal processing and
235 transmission. During neuronal development, the current density of I_{Na} amplifies, thereby
236 increasing the capacity of neurons to generate action potentials. Our results indicate a significant

237 increase in the magnitude of the I_{Na} from PCD105 to PCD155 (**Figure 4H**). This suggests that IT
238 neurons in the dlPFC acquire the ability to initiate and transmit APs after PCD105. In summary,
239 our analyses showed a progression in maturation across four distinct electrophysiological
240 properties. However, it is noteworthy that the temporal dynamics of the four electrophysiological
241 properties were not identical. While RMP and I_{Na} exhibited a progressive increase from PCD95-
242 100 to PCD155, C_m and R_{in} displayed drastic changes only at PCD105-110. Our study has
243 uncovered distinct profiles in the temporal dynamics of electrophysiological maturation, where
244 each property exhibits a different rate of maturation.

245 Similar to IT ExNs, InNs exhibited progressively more negative RMP and I_{Na} from
246 PCD105-110 to PCD155, whereas R_{in} didn't show any significant differences and C_m became
247 higher throughout development (**Figures S5A-S5E**). The proportion of InNs with APs increased
248 from 12.5% in PCD85-90 to 100% in PCD125, PCD145, and PCD155, indicating a faster
249 electrophysiological maturation than ExNs (**Figure S5F**).

250 We hypothesized that differential expression of distinct genes drives the divergent trends
251 of the four electrophysiological features across maturation. By implementing a correlation analysis
252 between the electrophysiological data and the gene expression levels across all IT neurons, we
253 identified 135, 163, 193, and 142 genes that are associated with the temporal dynamics of
254 electrophysiological features of C_m, R_{in}, RMP, and I_{Na}, respectively (**Figure S6A; Table S9**).
255 Importantly, genes that are not expected to exhibit correlation with electrophysiological features,
256 including the housekeeping genes *GAPDH* and *TBP*, showed no significant correlation with any
257 of the electrophysiological features (**Figure S6B**). Several genes, including *CAMK2A* and
258 *MICAL2*, exhibited high correlation with all four investigated electrophysiological features
259 (**Figures 4I-4L**). Other genes, such as *RAPGEF4*, exhibited significant correlation with one or two

260 of the electrophysiological features. To validate our Patch-seq data, we performed in situ
261 hybridization on dlPFC sections of PCD100 and PCD155 macaques for select genes that
262 demonstrated significant correlation with all (*CAMK2A*, *MICAL2*) or some (*RAPGEF4*, *NRGN*)
263 of the electrophysiological features. Consistent with the Patch-seq results, the expression levels of
264 all tested genes were significantly higher in PCD155 compared to PCD100 (**Figures 4D and S6C**).

265 Therefore, our Patch-seq analysis of dlPFC neurons across midfetal and late-fetal
266 development revealed evidence of neuronal maturation across three distinct aspects:
267 morphological, transcriptomic, and electrophysiological properties, and identified genes
268 associated with maturation of specific electrophysiological features.

269

270 ***RAPGEF4* is crucial for the morphological and electrophysiological maturation of excitatory**
271 **neurons**

272 Our Patch-seq analysis demonstrated a marked upregulation of *RAPGEF4* expression in IT
273 neurons during cortical development (**Figures 4K-4L**), which was also corroborated by our
274 snRNA-seq data (**Figure 5A**). RAPGEF4 (Rap Guanine Nucleotide Exchange Factor 4), also
275 known as EPAC2 (exchange protein directly activated by cyclic AMP 2), is a regulator of small
276 GTPase signaling and a protein kinase A (PKA)-independent cAMP target[37-39]. We found that
277 *RAPGEF4* expression exhibited a high degree of correlation with various electrophysiological
278 features, with the highest correlation observed with I_{Na} (r = -0.57) and the second highest
279 correlation with RMP (r = -0.47) (**Figure S6E**). To confirm that RAPGEF4 is required for neuronal
280 maturation, we infected ex vivo macaque brain slices with lentivirus (LV) expressing mScarlet
281 and shRNA against *RAPGEF4* (LV-sh*RAPGEF4*) together with LV expressing mNeonGreen and

282 control shRNA (LV-sh*NC*) (**Figure 5B**). The neurons with *RAPGEF4* knockdown (sh*RAPGEF4*,
283 mScarlet^{+}) exhibited reduced dendritic complexity, total dendritic length, branching points, and
284 number of endings compared to controls (mNeonGreen^{+}mScarlet^{-}) (**Figures 5C-5H**). In addition,
285 LV-sh*RAPGEF4*-infected neurons exhibited smaller I_{Na} (**Figures 5I and 5M**) and less negative
286 RMP (**Figures 5I and 5L**), without significant changes in C_m and R_{in}, compared to control neurons
287 (**Figures 5J-5K; Table S10**). These results indicate that a deficiency of *RAPGEF4* in neurons
288 leads to delayed maturation of I_{Na} and RMP, which is consistent with our finding that *RAPGEF4*
289 had a strong correlation with I_{Na} and RMP (**Figures 4K-4L and S6E**).

290 RAPGEF4 is enriched in neurons compared to other cell types[39]. The levels of *RAPGEF4*
291 increase in the human cortex throughout development, compared to other brain regions or
292 organs[9,40]. Based on our observations in macaque, we hypothesized that *RAPGEF4* expression is
293 also associated with the maturation of electrophysiological properties in human. We infected
294 human midfetal cortical brain slices with LV-sh*RAPGEF4* and performed patch-clamp recording.
295 As in macaque, we observed reduced I_{Na} and RMP, but not C_m and R_{in}, in LV-sh*RAPGEF4*-
296 infected compared to LV-sh*NC*-infected neurons (**Figures 5N-5R; Table S10**). To confirm that
297 the observed effect was not caused by off-target effects of the shRNA, we replicated the
298 experiment and observed the same results using a different shRNA targeting *RAPGEF4* in human
299 neurons (**Figures S6H-S6L**). The role of RAPGEF4 in regulating RMP and I_{Na} maturation in both
300 macaque and human neurons is consistent with the functional enrichment for "regulation of
301 GTPase activity" in genes driving neuronal maturation (**Figure S6D**). These data validate our
302 approach to identify genes that drive the maturation of specific electrophysiological features and
303 reveal the novel role of *RAPGEF4* in morphological and electrophysiological maturation of
304 neurons in both macaque and human cortical development.

305

306 ***CHD8* knockdown leads to impaired maturation of human cortical excitatory neurons**

307 Recent advances in genomics have revealed important roles of chromatin regulators during
308 midfetal PFC development and implicated them in neurodevelopmental disorders[41,42]. CHD8
309 (Chromodomain Helicase DNA-binding protein 8) is a chromatin remodeling protein that plays a
310 crucial role in regulating gene expression during brain development and has been linked to ASD[42-
311 44]. To investigate the role of *CHD8* during human midfetal cortical development, a critical
312 developmental period for ASD[14,15], we knocked down *CHD8* expression in ex vivo human
313 midfetal brain slices using LV expressing sh*CHD8* and mScarlet together with LV expressing
314 *shNC* and mNeonGreen (**Figures 6A and S7B-S7C**). LV-sh*CHD8*-infected neurons displayed
315 significantly shorter dendrites compared to control neurons (**Figures 6B, 6D-6E and S7D-S7F**),
316 suggesting that a deficiency in *CHD8* disrupts morphological maturation of cortical neurons during
317 midfetal development, which is consistent with previous findings in mice[44].

318 We then performed Patch-seq on 156 cells from slices that contained both *CHD8*-
319 knockdown and control cells (**Figures 6A and S7G**). To determine the cellular identity of recorded
320 cells, we compared their transcriptome with the reference snRNA-seq data and assigned each
321 queried cell a specific cell type (**Figures 6C and S7H; Table S11**). Out of the 156 cells examined,
322 there were 55 excitatory neurons infected with LV-sh*NC* and 42 infected with LV-sh*CHD8* (**Table**
323 **S11**). LV-sh*CHD8*-infected excitatory neurons had less negative RMP and a significant increase
324 in R_{in} (**Figures 6I and 6H**) but not in C_m and I_{Na} (**Figures 6G, 6J and S7I**), compared to the
325 controls. To rule out the possibility that the observed effect is due to shRNA off-target effects, we
326 repeated the experiment with an alternative shRNA in human cultured neurons and observed
327 similar deficits in both R_{in} and RMP (**Figures S7J-S7N**). Therefore, *CHD8* knockdown produces

328 a discernible impact on the electrophysiological properties of midfetal human neurons, which is
329 consistent with its role during early development[43,44].

330

331 **RAPGEF4 rescues electrophysiological deficits of CHD8-deficient human cortical neurons**

332 To determine which genes might underlie the observed differences in R_{in} and RMP maturation
333 caused by *CHD8* knockdown, we identified the differentially expressed genes between LV-
334 sh*CHD8* and LV-sh*NC* and intersected this list with the genes that were associated with the
335 maturation of these two electrophysiological features (**Table S9**). We found 10 genes associated
336 with R_{in}, 11 genes associated with RMP, and 20 genes associated with both (**Figure 7A**). These
337 included genes that are associated with the overall maturation of neurons, such as *NRGN* and
338 *CACNA1I*, the R_{in}-associated *RGS6*, a GTPase regulator important for activity-dependent
339 morphological and electrical maturation[45], and *RAPGEF4*, which we found to significantly impact
340 the maturation of RMP (**Figures 7B-7E and 5**).

341 To determine whether reduced RAPGEF4 levels might contribute to the observed reduced
342 RMP in *CHD8* deficient neurons, we expressed *RAPGEF4* in human cortical neurons that were
343 knockdown for *CHD8* (sh*CHD8*) (**Figure 7F**). Exogenously expressed *RAPGEF4* restored normal
344 maturation of both RMP and I_{Na}, with no significant effect on R_{in} or C_m, in *CHD8*-deficient neurons
345 (**Figures 7G-7L; ; Table S12**). Therefore, *CHD8* deficiency in primate cortical neurons leads to
346 reduced expression of genes important for electrophysiological maturation, including *RAPGEF4*,
347 which may contribute to neuronal maturation deficits.

348

349 **DISCUSSION**

350 In this study, we employed multimodal approaches including snMultiome and Patch-seq to
351 interrogate mechanisms driving neuronal maturation in the primate dlPFC during midfetal and
352 late-fetal development. We identified dynamic gene expression changes across cell types in their
353 maturation trajectories as well as critical developmental periods for the maturation of specific
354 electrophysiological properties in excitatory and inhibitory neurons.

355 We confirmed that, based on their molecular profiles, excitatory neurons gain their laminar
356 and projection identities earlier than interneuronal final specification. This corroborates previous
357 findings that pointed to the relevance of extrinsic factors to the final specification of interneurons
358 during perinatal development[20,45]. We focused our analyses on the IT excitatory neurons due to
359 their relevance both to primate brain evolution and their association to neuropsychiatric disorders.
360 Our integrative analysis of gene expression and chromatin accessibility data unveiled gene
361 regulatory networks associated with neuron maturation of both excitatory and inhibitory neurons
362 and highlighted MEIS2 as a key transcriptional factor for L2-3 IT neuronal development and
363 maturation.

364 By integrating electrophysiology, morphology, and functional genomics analyses of
365 primate dlPFC development, we discovered that different electrophysiological properties mature
366 at different rates. While RMP change gradually and linearly during maturation, C_m and R_{in} exhibit
367 a jump at the end of neurogenesis during midfetal developmental, I_{Na} exhibited significant
368 maturation only at the late-fetal period, which coincides with a significant increase in the number
369 of neurons able to fire action potentials. The distinct rate of maturation among electrophysiological
370 properties reveals the intricate and finely tuned regulation of neuronal maturation during midfetal
371 and late-fetal development of primate PFC.

372 Our Patch-seq approach allowed us to investigate the genes associated with the maturation
373 of specific electrophysiological features. We have uncovered genes, including kinases, small GTP
374 signaling molecules, neurotransmitter receptors, ion channels, and transporters that are associated
375 with maturation of specific electrophysiological features that likely underlie the differences we
376 observed in their maturation kinetics. One of these genes is *RAPGEF4*, which we have identified
377 as being significantly correlated with the maturation of resting membrane potentials and inward
378 sodium currents. RAPGEF4, a guanine exchange factor in small GTPase pathway, is a direct target
379 of cAMP and has been shown to regulate dendritic spine remodeling in mice and its deficiency in
380 mice leads to learning and memory deficits[39,46]. However, its role in primate brain development or
381 human disease is unknown. Dysregulation of the cAMP pathway has been implicated in a wide
382 range of neurological disorders and a potential treatment to elevate cAMP levels is currently in
383 clinical trial for fragile X syndrome[47-49]. The small GTPase pathway has been shown to have
384 critical roles during maturation of human neurons[50]. Our study demonstrates that RAPGEF4 may
385 be one of the small GTPase regulators driving neuronal maturation during primate brain
386 development, especially for RMP, an electrophysiological feature regulated by GTPase signaling.

387 Finally, to demonstrate the potential of our experimental platform in exploring the
388 developmental origin of human diseases, we showed that knocking down of a high-confidence
389 ASD gene – *CHD8* – impaired morphological and electrophysiological maturation of excitatory
390 neurons in human organotypic slices. This impairment was driven by the downregulation of the
391 expression of several key genes that we identified to be relevant for the electrophysiological
392 maturation of neurons, including *RAPGEF4 and RGS6*, two regulators of small GTPase signaling
393 critical for neuronal maturation[50]. By restoring the expression of *RAPGEF4* in CHD8-deficient
394 neurons we were able to rescue the deficits in electrophysiological maturation of these neurons.

395 The chromatin regulator CHD8 is expressed at high levels during early-fetal and midfetal
396 development and the levels of CHD8 do not exhibit significant upregulation during midfetal to
397 late-fetal neuronal maturation. How CHD8 and other early expressing chromatin regulators
398 converging at midfetal development contribute to ASD remains unclear. Our finding sheds light
399 on how a chromatin remodeler may regulate the physiological maturation of neurons, thus
400 impairing their normal functioning.

401 Together, our study has revealed key genes and gene networks driving neuronal maturation
402 during a critical period of prefrontal development in primates and linked the function of a novel
403 regulator of the maturation of specific electrophysiological features with a high-confidence ASD
404 risk gene. Our results demonstrate the power of our multimodal approach and its application for
405 future studies aiming at understanding how genes regulate neuronal maturation and its implication
406 in brain disorders. Finally, we summarized our results including cell clusters, genes and networks
407 in an open-access, searchable web app, which will allow researchers to investigate the role of
408 different genes on neuronal maturation.

409

410 **ACKNOWLEDGEMENTS**

411

412 We thank Y. Xing, S. Krebsbach, D. Phan, M. Weidenfeller, and H. Thurston for technical
413 assistance; K. Knobel at the Waisman IDD Model Core for core services; Dr. Heather Simmons,
414 Director of Pathology Services (WNPRC) for non-human primate tissue acquisition; and the Birth
415 Defects Research Laboratory (BDRL) at the University of Washington for human tissue
416 acquisition. This work was supported by the National Institutes of Health (R01MH118827 and
417 R01NS105200 to X.Z.; R01HD064743 to Q.C; R01NS064025, R01AG067025, and
418 RF1MH128695 to D.W; 1R01HD106197 and UM1MH130991 to A.M.M.S; P51 OD011106 to

WNPRC; P50HD105353 to Waisman Center; and R24HD000836 to BDRL). Further support was provided by the DOD IIRA grant (X.Z.), SFARI pilot grant (X.Z., A.M.M.S., Q.C., and D.W.), Jenni and Kyle Professorship (X.Z.), Brain and Behavior Research Foundation (29721 to A.M.M.S.), Brain Research Foundation (BRFSG-2023-11 to A.M.M.S.), and the Medical Scientist Training Program T32 (GM140935 to R.D.R.).

AUTHOR CONTRIBUTIONS

Y.G., Q.D., Q.C., X.Z., and A.M.M.S. conceived and designed the study. Y.G., Q.D., R.D.R., M.S., D.K.S., and A.M.M.S. performed the experiments. K.H.A., J.S., T.J., S.L., S.K., and D.W. analyzed the genomics data. J.E.L., D.D., I.G. provided the analyzed specimens. Y.G., Q.D., K.H.A., Q.C., X.Z., and A.M.M.S. wrote the manuscript. All authors edited the manuscript.

DECLARATION OF INTERESTS

The authors declare no competing interests.

RESOURCE AVAILABILITY

The genomic data has been submitted to GEO (GSE235493). The data can be interactively visualized at https://daifengwanglab.shinyapps.io/DevMacaquePFC/. The code and data used for generating figures can be accessed at Zenodo: https://zenodo.org/records/11123264. All other data are available in the main article or supplemental information. Further information and requests for resources should be directed to the corresponding authors.

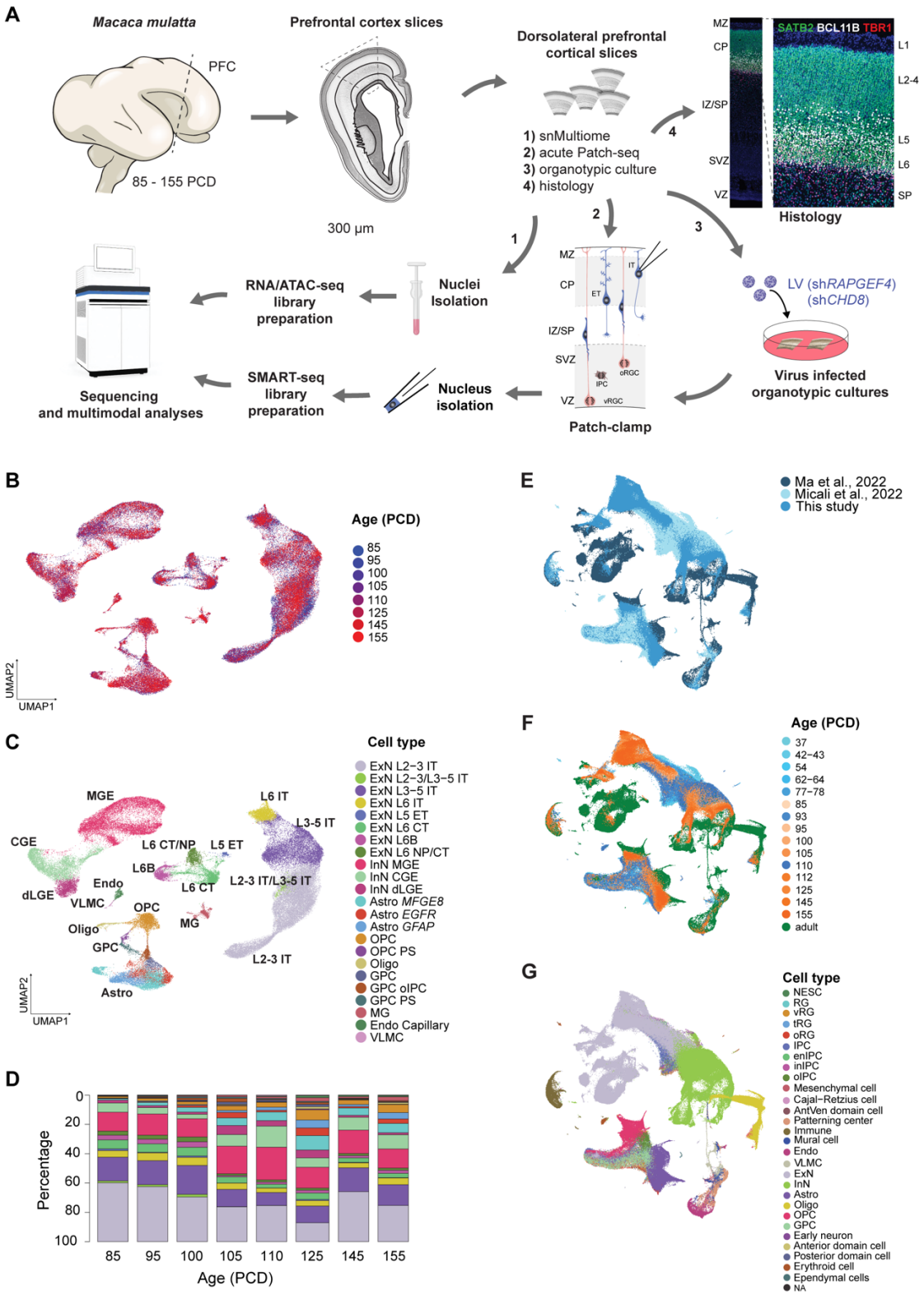

Figure 1. Single-nucleus transcriptomic atlas of rhesus macaque dlPFC cells across midfetal and late-fetal development

444 (A) The frontal cortex of Rhesus macaque (*Macaca mulatta*) brains, aged from postconceptional
445 day (PCD) 85 to 155, were dissected and sectioned at 300 μm. Acute dorsolateral prefrontal
446 cortices were analyzed using Patch-seq and single-nucleus multiome (snRNA-seq and snATAC-
447 seq). Tissue from the same specimens, as well as human midfetal tissue, was also used to culture
448 organotypic slices for functional analyses of select genes (*RAPGEF4* and *CHD8*). Validation of
449 key findings was also performed by multiplexed immunostaining and single-molecule fluorescent
450 in situ hybridization on dlPFC sections from the contralateral hemisphere of the same specimens
451 (**Table S1**). Finally, we have performed an integrative analysis of the generated multimodal
452 dataset.
453 (B-C) UMAP visualization of all the cell classes and subclasses. Cells are colored according to
454 age in postconceptional days (PCD), from PCD85-PCD155 (B) cell subclass (C).
455 (D) Bar plot showing the cell composition of the dlPFC throughout midfetal and late-fetal
456 development.
457 (E-G) Integrated UMAP visualization depicting cells obtained from both the current study and
458 published datasets[22,27]. Cells are color-coded based on their respective dataset (current study in
459 medium blue) (E), age of donor specimen (embryonic/early fetal in blue, current study in orange,
460 adult in dark green) (F), and cell type (G). ExN, excitatory neuron; InN, inhibitory neurons; Astro,
461 astrocytes; Oligo, oligodendrocytes; IPC, intermediate precursor cells; enIPC, excitatory neuron
462 IPC; inIPC inhibitory neuron IPC; oIPC, oligodendrocyte IPC; OPC, oligodendrocyte precursor
463 cells; GPC, glial precursor cells; Endo, endothelial cells; RG, radial glia cells; oRG, outer radial
464 glia cells; tRG, truncated radial glia cells; vRG, ventricular radial glia cells; NESC, neuroepithelial
465 stem cells; VLMC, vascular leptomeningeal cells; AntVen domain cell, antero-ventral domain
466 cells; NA, unknown cell type.

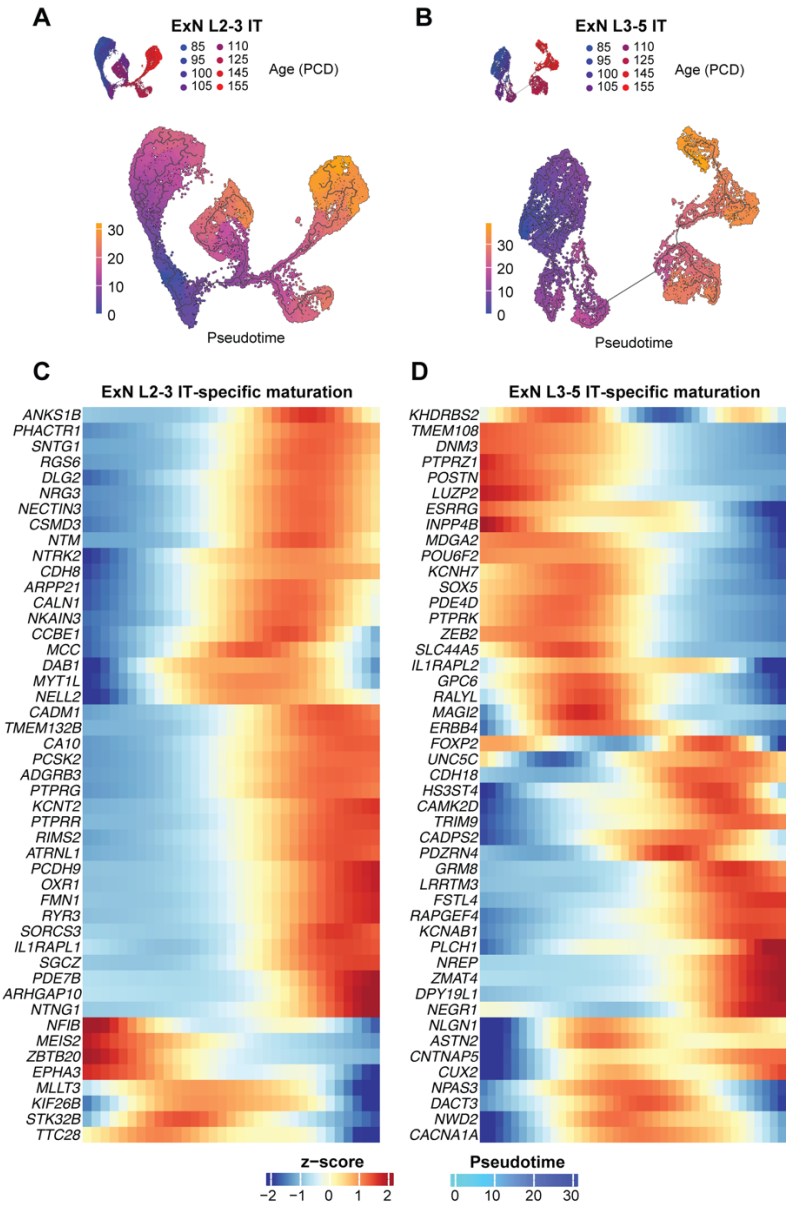

Figure 2. Maturational trajectories of L2-3 and L3-5 intratelencephalic-projecting neurons. (A-B) UMAP visualization of the maturation trajectory of ExN L2-3 IT (A), and ExN L3-5 IT (B) cells; the top panel is colored according to postconceptional days, whereas the bottom panel is colored according to inferred pseudotime.

(C-D) Gene expression variation with pseudotime of genes specific to ExN L2-3 IT (C), ExN L3-5 IT (D) (from the top 100 highly variable genes along the developmental trajectory).

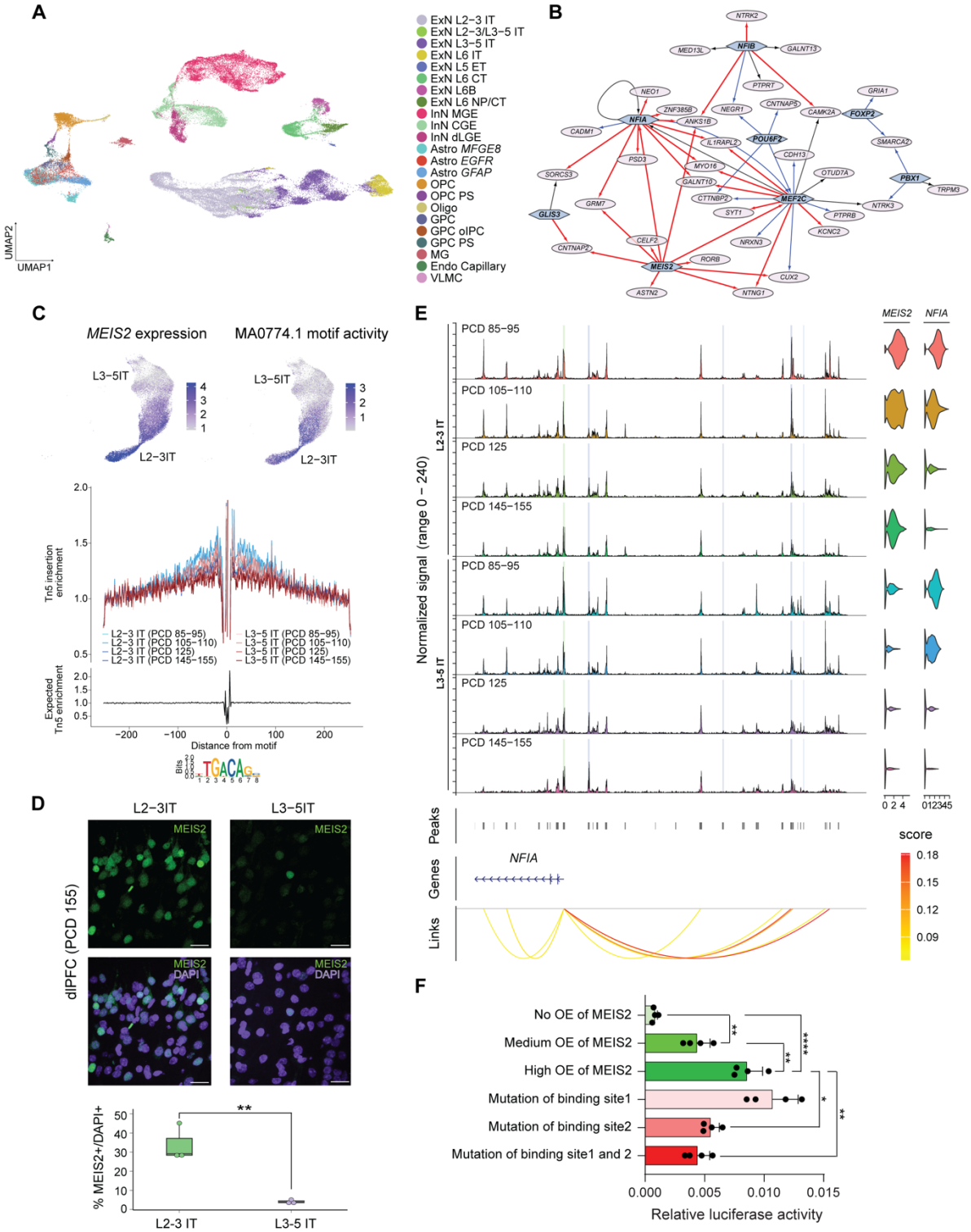

Figure 3. Single-nucleus multiome gene expression and chromatin accessibility of rhesus macaque dlPFC cells across mid- to late-fetal development.

478 (A) Joint (snRNA-seq and snATAC-seq) UMAP visualization of cell subclasses.

479 (B) Differential gene regulatory networks inferred for ExN L2-3 IT and ExN L3-5 IT cell
480 subclasses. Hexagonal nodes indicate transcription factors, and the elliptical nodes indicate the
481 target genes. The edge colors represent the cell subclass specificity of transcription factor-target
482 gene relationships (black, conserved in both cell subclasses; red, ExN L2-3 IT specific; blue, ExN
483 L3-5 IT specific).

484 (C) UMAP visualization of *MEIS2* expression and motif activity scores for MA0774.1 (MEIS2
485 transcription factor motif) in L2-3 IT and L3-5 IT cells (top panels); MEIS2 transcription factor
486 footprints for ExN L2-3 IT and ExN L3-5 IT cells across four developmental periods (bottom
487 panel).

488 (D) Immunofluorescent detection of MEIS2 in the macaque dlPFC at PCD155, in L2-3 IT and L3-
489 5 IT cells shows that a significantly higher number of cells express MEIS2 in L2-3 IT than in L3-
490 5 IT cells (L3-5 was identified using in situ hybridization against *RORB*, as shown in Figure S3E).
491 Scale bar, 20 μm. (**$p < 0.01$, *t*-test).

492 (E) Peak-to-gene link plot for *NFIA* together with the gene expression of *MEIS2* and *NFIA* in ExN
493 L2-3 IT and ExN L3-5 IT across four developmental periods. The links indicate the co-activity
494 links between *NFIA* gene expression and chromatin accessibility peaks. The highlighted regions
495 within the chromatin accessibility peaks show the MEIS2 transcription factor motif (MA0774.1)
496 binding sites.

497 (F) Dual-Luciferase reporter assay of *NFIA* genomic sequences containing MEIS2 motifs. OE,
498 overexpression. *$p < 0.05$, **$p < 0.01$, ****$p < 0.0001$ (one-way analysis of variance with Tukey
499 multiple comparisons). Each dot represents one replicate.

500

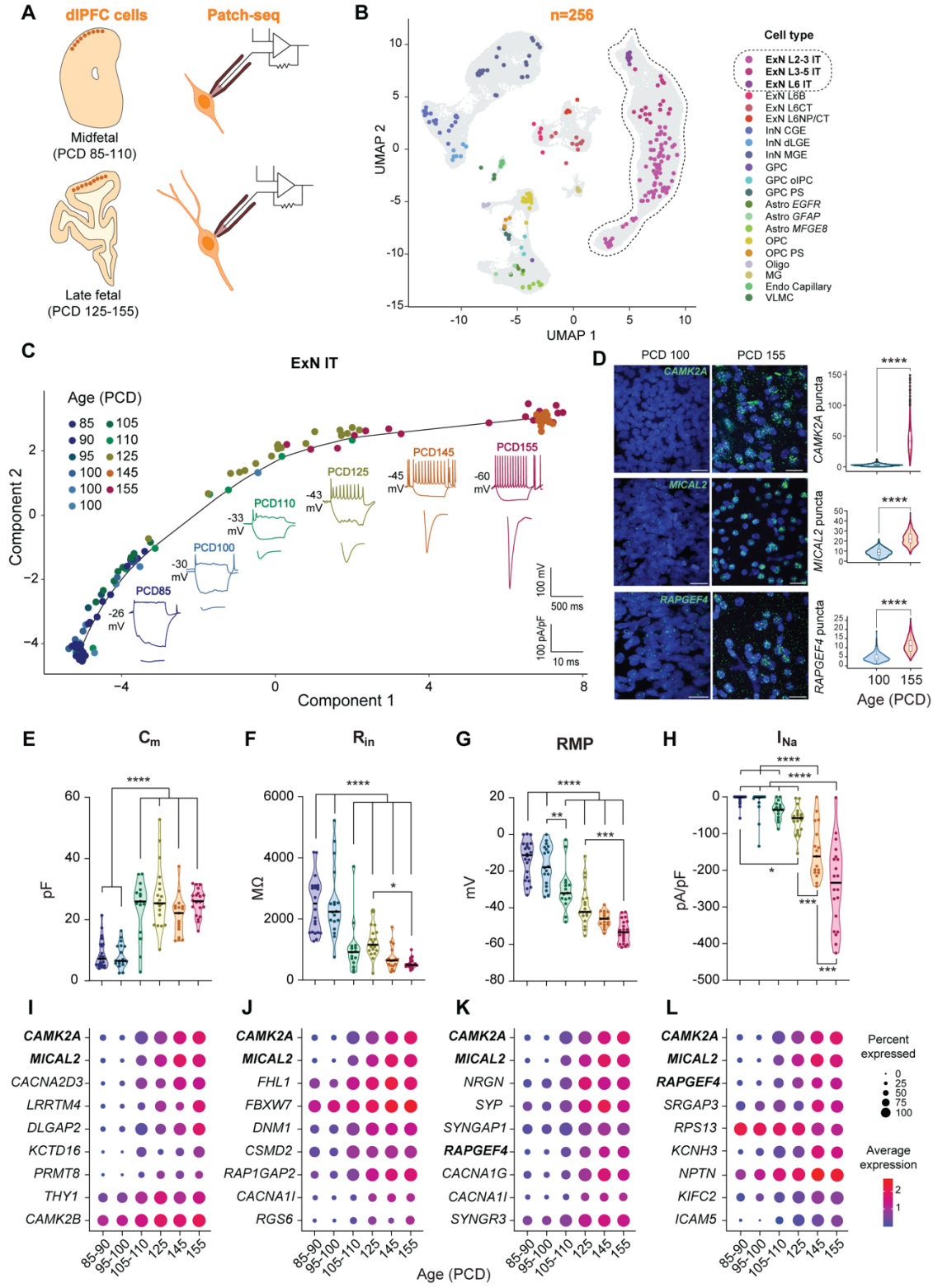

Figure 4. Identification of midfetal and late-fetal neuronal maturation-related genes using Patch-seq.

504 (A) Schematic representation of the Patch-seq experimental design for analyzing midfetal and late-
505 fetal rhesus macaque dlPFC cells.
506 (B) Integration of the 256 cells profiled by Patch-seq onto the snRNA-seq reference UMAP.
507 (C) Pseudotime trajectory based on the gene expression profiles of patched IT neurons from 16
508 individual rhesus macaque fetal brains at 9 distinct fetal ages, with representative
509 electrophysiological sample traces (voltage responses to depolarizing and hyperpolarizing current
510 injections, and inward sodium currents).
511 (D) In situ hybridization detection and quantification (right panel) of *CAMK2A*, *MICAL2*, and
512 *RAPGEF4* in PCD100 and PCD155 dlPFC. Scale bar, 20 µm. (****$p < 0.0001$, *t*-test).
513 (E-L) Plots illustrating the developmental changes in electrophysiological properties, including
514 membrane capacitance (C_m, E), input resistance (R_{in}, F), resting membrane potential (RMP, G),
515 and inward sodium current (I_{Na}, H) of IT neurons across six different age groups. Bottom panels
516 show the expression levels of C_m-correlated genes (I), R_{in}-correlated genes (J), RMP-correlated
517 genes (K), and I_{Na}-correlated genes (L) in IT neurons across the same age groups. (**$p < 0.01$,
518 ***$p < 0.001$, ****$p < 0.0001$, one-way ANOVA, Tukey's multiple comparisons test).
519
520
521
522
523
524
525
526

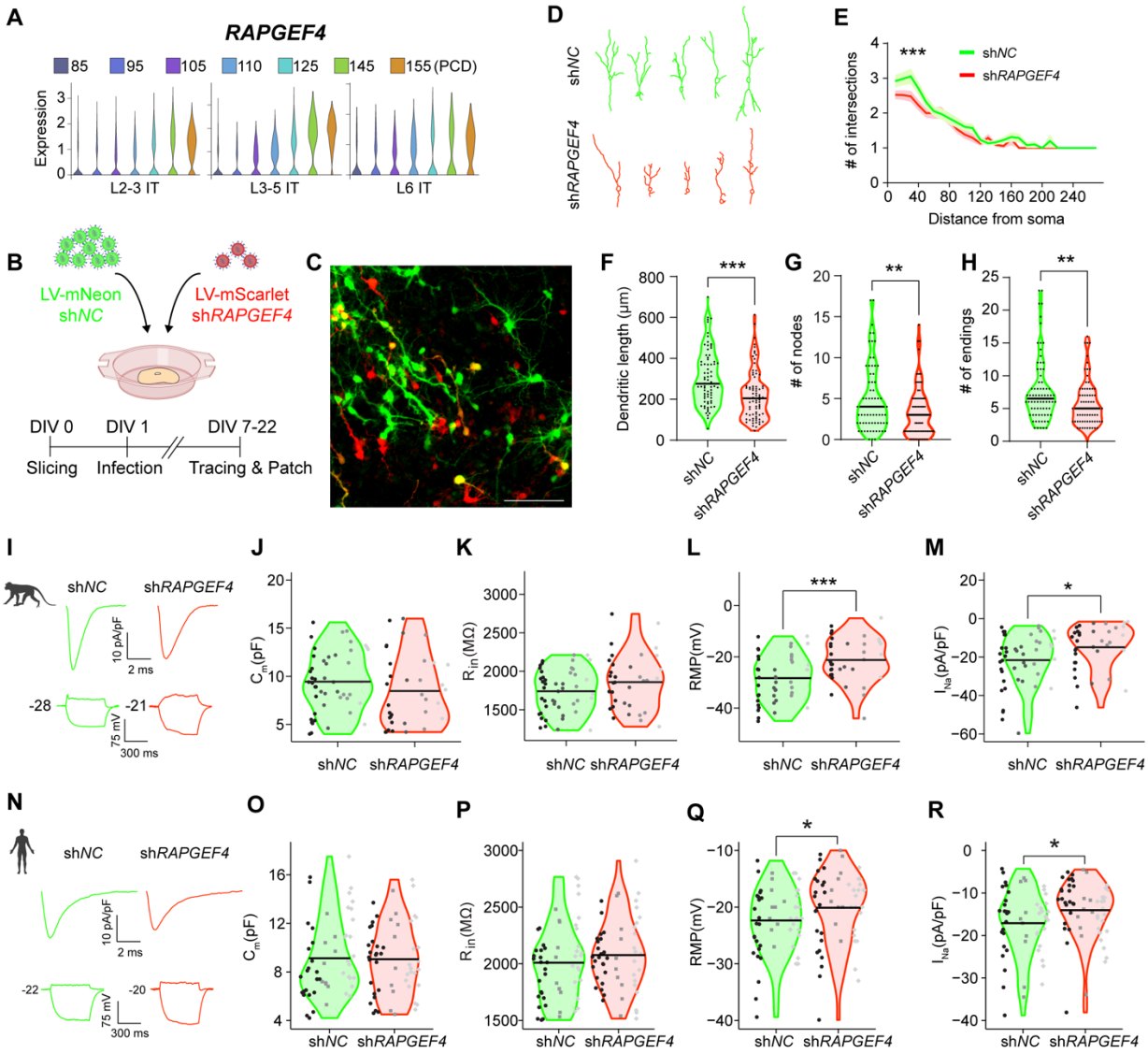

Figure 5. Knockdown of *RAPGEF4* impairs morphological and electrophysiological maturation of cortical neurons in macaque organotypic dlPFC slices.

(A) Violin plots showing the expression of *RAPGEF4* in IT neurons from PCD85 to PCD155.

(B) Schematic of the experimental setup for investigating the morphological and electrophysiological alterations after *RAPGEF4* knockdown in ex vivo dlPFC slices.

(C) Representative image depicting *RAPGEF4* knockdown (both mScarlet^{+}[red] and mScarlet^{+}/mNeon^{+}[yellow]) and control (mNeon^{+}[green only]) neurons in macaque dlPFC slices. Scale bar, 100 μm.

536 (D) Sample traces depicting the morphology of both *RAPGEF4* knockdown (bottom panel) and
537 control (top panel) neurons.
538 (E) Sholl analysis of dendritic complexity in *RAPGEF4* knockdown neurons compared to control
539 neurons [$F(1,150) = 14.531$, ***$p < 0.001$, multivariate analysis of variance].
540 (F-H) Knockdown of *RAPGEF4* decreases total dendritic length (F), number of nodes (G), and
541 number of endings (H) (*t*-test, ***$p < 0.001$, **$p < 0.01$).
542 (I) Representative traces of inward sodium currents and voltage responses to depolarizing and
543 hyperpolarizing current injections for macaque *RAPGEF4* knockdown (right panel) and control
544 (left panel) neurons.
545 (J-M) Knockdown of *RAPGEF4* in macaque organotypic slices leads to reduced I_{Na} (M) and less
546 negative RMP (L), without significantly change in C_m (J) and R_{in} (K) (*t*-test, ***$p < 0.001$, *$p <$
547 0.05). Each dot represents one patched cell. All cells were collected from four individual fetal
548 brains, with each fetal brain indicated by a different color: black, dark gray, medium gray, and
549 light gray.
550 (N) Representative traces of inward sodium currents and voltage responses to depolarizing and
551 hyperpolarizing current injections for human *RAPGEF4* knockdown (right panel) and control (left
552 panel) neurons.
553 (O-R**)** Knockdown of *RAPGEF4* in human organotypic slices leads to reduced I_{Na} (R) and less
554 negative RMP (Q), without significantly change in C_m (O) and R_{in} (P) (*$p < 0.05$). Each dot
555 represents one patched cell. All cells were collected from four individual fetal brains, with each
556 fetal brain indicated by a different color: black, dark gray, medium gray, and light gray.
557

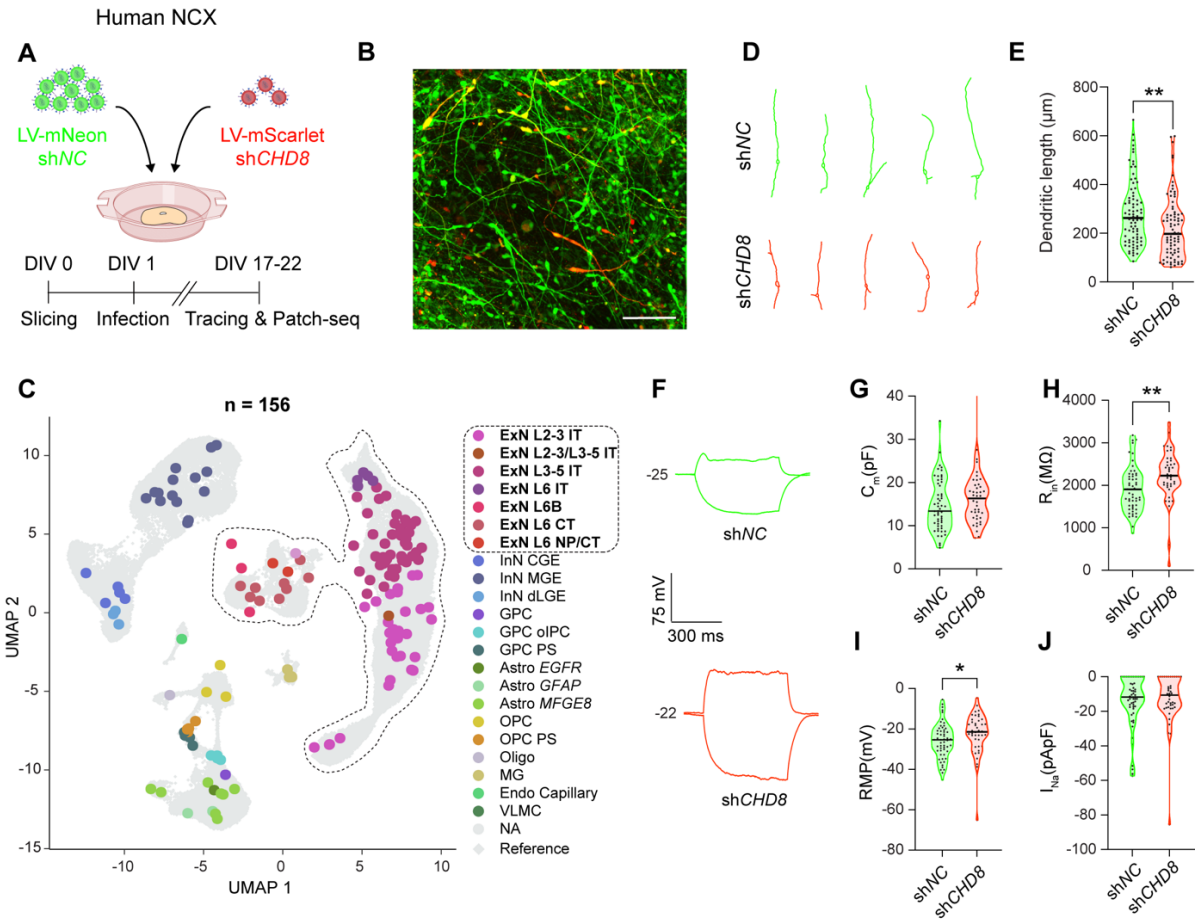

Figure 6. Knockdown of *CHD8* impairs maturation of cortical excitatory neurons.

(A) Schematic diagram illustrating the experimental setup used to study the morphological and electrophysiological changes after knockdown of *CHD8* in ex vivo human fetal cortical slices.

(B) Representative image showing *CHD8* knockdown (mScarlet^{+}[red], mScarlet^{+} and mNeon^{+}[yellow]) and control (mNeon^{+}[green]) neurons in human cortical slices. Scale bar, 100 μm.

(C) Integration of the 156 cells profiled by Patch-seq onto the snRNA-seq reference UMAP.

(D) Sample traces showing the morphology of both *CHD8* knockdown and control neurons.

(E) *CHD8* knockdown reduces total dendritic length (**$p < 0.01$, *t*-test).

(F) Representative traces (voltage response to depolarizing [50 pA] and hyperpolarizing [-50 pA] current injections) for control neurons and *CHD8* knockdown.

570 (G-J) *CHD8* knockdown increases R_{in} (H) and RMP (I) but does not significantly alter C_m (G) and

571 I_{Na} (J) (*p < 0.05, **p < 0.01, *t*-test).

572

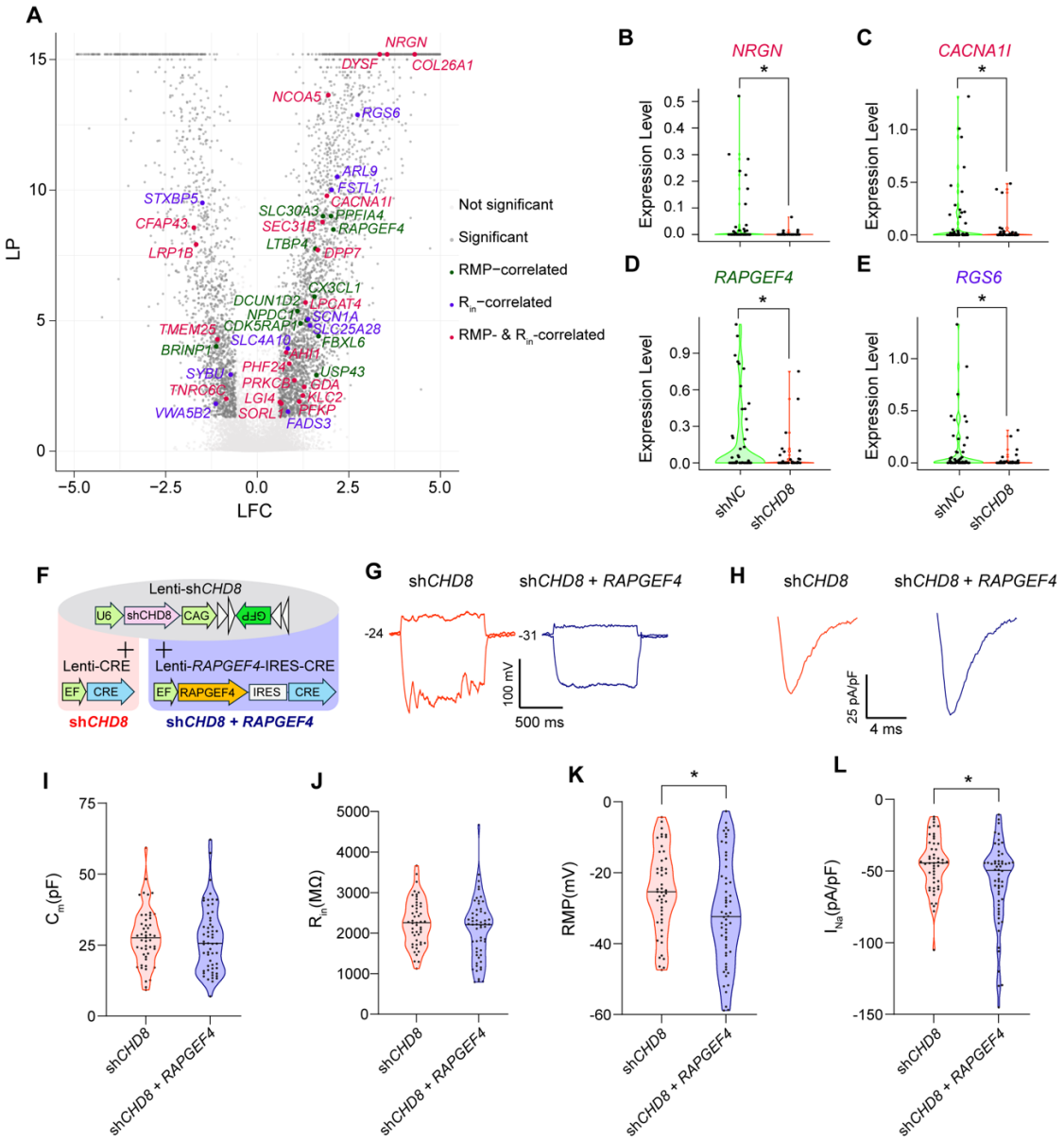

573

574 **Figure 7. Exogenously expressed RAPGEF rescues neuronal maturation deficits resulting**

575 **from CHD8 deficiency.**

576 (A) Volcano plot depiction ($-\log_{10}(P_{adj})$ vs $\log_2$(*fold-change*)) of differentially expressed genes

577 between LV-sh*NC* and LV-sh*CHD8* -infected excitatory neurons. Genes with expression profiles

578 that significantly correlate with the RMP (green), R_{in} (purple), or both (red) electrophysiology
579 features are labeled.
580 (B-E) Violin plots showing the expression levels of *NRGN* (B), *CACNA1I* (C), *RAPGEF4* (D), and
581 *RGS6* (E), highlighting the effect of *CHD8* knockdown on these neuronal maturation genes
582 (Figures 4I-4L).
583 (F) Schematic of lentiviral vectors used for knocking down *CHD8* and overexpression of
584 *RAPGEF4* in human cortical ex vivo organotypic slices.
585 (G) Representative traces (voltage response to depolarizing [50 pA] and hyperpolarizing [-50 pA]
586 current injections) for neurons with *CHD8* knockdown and neurons with *CHD8* knockdown and
587 *RAPGEF4* overexpression.
588 (H) Representative traces of inward sodium currents to depolarizing current injections for neurons
589 with *CHD8* knockdown and neurons with *CHD8* knockdown and *RAPGEF4* overexpression.
590 (I-L) *RAPGEF4* rescues RMP (K) and I_{Na} (L) but does not significantly alter C_m (I) and R_{in} (J) of
591 neurons with *CHD8* knockdown (*$p < 0.05$, **$p < 0.01$, *t*-test).
592
593 **REFERENCES**

594 1. Preuss, T.M., and Wise, S.P. (2022). Evolution of prefrontal cortex.
595 Neuropsychopharmacology *47*, 3-19. 10.1038/s41386-021-01076-5.
596 2. Smaers, J.B., Gomez-Robles, A., Parks, A.N., and Sherwood, C.C. (2017). Exceptional
597 Evolutionary Expansion of Prefrontal Cortex in Great Apes and Humans. Curr Biol *27*,
598 1549. 10.1016/j.cub.2017.05.015.
599 3. Sousa, A.M.M., Meyer, K.A., Santpere, G., Gulden, F.O., and Sestan, N. (2017). Evolution
600 of the Human Nervous System Function, Structure, and Development. Cell *170*, 226-247.
601 10.1016/j.cell.2017.06.036.
602 4. Levy, R., and Goldman-Rakic, P.S. (1999). Association of storage and processing
603 functions in the dorsolateral prefrontal cortex of the nonhuman primate. J Neurosci *19*,
604 5149-5158. 10.1523/JNEUROSCI.19-12-05149.1999.
605 5. Kritzer, M.F., and Goldman-Rakic, P.S. (1995). Intrinsic circuit organization of the major
606 layers and sublayers of the dorsolateral prefrontal cortex in the rhesus monkey. J Comp
607 Neurol *359*, 131-143. 10.1002/cne.903590109.

6. Lewis, D.A., and Mirnics, K. (2006). Transcriptome alterations in schizophrenia: disturbing the functional architecture of the dorsolateral prefrontal cortex. Prog Brain Res *158*, 141-152. 10.1016/S0079-6123(06)58007-0.
7. Cools, R., and Arnsten, A.F.T. (2022). Neuromodulation of prefrontal cortex cognitive function in primates: the powerful roles of monoamines and acetylcholine. Neuropsychopharmacology *47*, 309-328. 10.1038/s41386-021-01100-8.
8. Pattabiraman, K., Muchnik, S.K., and Sestan, N. (2020). The evolution of the human brain and disease susceptibility. Curr Opin Genet Dev *65*, 91-97. 10.1016/j.gde.2020.05.004.
9. Zhu, Y., Sousa, A.M.M., Gao, T., Skarica, M., Li, M., Santpere, G., Esteller-Cucala, P., Juan, D., Ferrandez-Peral, L., Gulden, F.O., et al. (2018). Spatiotemporal transcriptomic divergence across human and macaque brain development. Science *362*. 10.1126/science.aat8077.
10. Shibata, M., Pattabiraman, K., Lorente-Galdos, B., Andrijevic, D., Kim, S.K., Kaur, N., Muchnik, S.K., Xing, X., Santpere, G., Sousa, A.M.M., and Sestan, N. (2021). Regulation of prefrontal patterning and connectivity by retinoic acid. Nature *598*, 483-488. 10.1038/s41586-021-03953-x.
11. Shibata, M., Pattabiraman, K., Muchnik, S.K., Kaur, N., Morozov, Y.M., Cheng, X., Waxman, S.G., and Sestan, N. (2021). Hominini-specific regulation of CBLN2 increases prefrontal spinogenesis. Nature *598*, 489-494. 10.1038/s41586-021-03952-y.
12. Pletikos, M., Sousa, A.M., Sedmak, G., Meyer, K.A., Zhu, Y., Cheng, F., Li, M., Kawasawa, Y.I., and Sestan, N. (2014). Temporal specification and bilaterality of human neocortical topographic gene expression. Neuron *81*, 321-332. 10.1016/j.neuron.2013.11.018.
13. Silbereis, J.C., Pochareddy, S., Zhu, Y., Li, M., and Sestan, N. (2016). The Cellular and Molecular Landscapes of the Developing Human Central Nervous System. Neuron *89*, 248-268. 10.1016/j.neuron.2015.12.008.
14. Willsey, A.J., Sanders, S.J., Li, M., Dong, S., Tebbenkamp, A.T., Muhle, R.A., Reilly, S.K., Lin, L., Fertuzinhos, S., Miller, J.A., et al. (2013). Coexpression networks implicate human midfetal deep cortical projection neurons in the pathogenesis of autism. Cell *155*, 997-1007. 10.1016/j.cell.2013.10.020.
15. Parikshak, N.N., Luo, R., Zhang, A., Won, H., Lowe, J.K., Chandran, V., Horvath, S., and Geschwind, D.H. (2013). Integrative functional genomic analyses implicate specific molecular pathways and circuits in autism. Cell *155*, 1008-1021. 10.1016/j.cell.2013.10.031.
16. Schmitz, M.T., Sandoval, K., Chen, C.P., Mostajo-Radji, M.A., Seeley, W.W., Nowakowski, T.J., Ye, C.J., Paredes, M.F., and Pollen, A.A. (2022). The development and evolution of inhibitory neurons in primate cerebrum. Nature *603*, 871-877. 10.1038/s41586-022-04510-w.
17. Nowakowski, T.J., Bhaduri, A., Pollen, A.A., Alvarado, B., Mostajo-Radji, M.A., Di Lullo, E., Haeussler, M., Sandoval-Espinosa, C., Liu, S.J., Velmeshev, D., et al. (2017). Spatiotemporal gene expression trajectories reveal developmental hierarchies of the human cortex. Science *358*, 1318-1323. 10.1126/science.aap8809.
18. Bhaduri, A., Sandoval-Espinosa, C., Otero-Garcia, M., Oh, I., Yin, R., Eze, U.C., Nowakowski, T.J., and Kriegstein, A.R. (2021). An atlas of cortical arealization identifies dynamic molecular signatures. Nature *598*, 200-204. 10.1038/s41586-021-03910-8.

19. Johnson, M.B., and Walsh, C.A. (2017). Cerebral cortical neuron diversity and development at single-cell resolution. Curr Opin Neurobiol *42*, 9-16. 10.1016/j.conb.2016.11.001.
20. Lim, L., Mi, D., Llorca, A., and Marin, O. (2018). Development and Functional Diversification of Cortical Interneurons. Neuron *100*, 294-313. 10.1016/j.neuron.2018.10.009.
21. Bandler, R.C., Mayer, C., and Fishell, G. (2017). Cortical interneuron specification: the juncture of genes, time and geometry. Curr Opin Neurobiol *42*, 17-24. 10.1016/j.conb.2016.10.003.
22. Molyneaux, B.J., Arlotta, P., Menezes, J.R.L., and Macklis, J.D. (2007). Neuronal subtype specification in the cerebral cortex. Nat Rev Neurosci *8*, 427-437. Doi 10.1038/Nrn2151.
23. Ma, S., Skarica, M., Li, Q., Xu, C., Risgaard, R.D., Tebbenkamp, A.T.N., Mato-Blanco, X., Kovner, R., Krsnik, Z., de Martin, X., et al. (2022). Molecular and cellular evolution of the primate dorsolateral prefrontal cortex. Science *377*, eabo7257. 10.1126/science.abo7257.
24. Berg, J., Sorensen, S.A., Ting, J.T., Miller, J.A., Chartrand, T., Buchin, A., Bakken, T.E., Budzillo, A., Dee, N., Ding, S.L., et al. (2021). Human neocortical expansion involves glutamatergic neuron diversification. Nature *598*, 151-158. 10.1038/s41586-021-03813-8.
25. Krienen, F.M., Goldman, M., Zhang, Q., R, C.H.D.R., Florio, M., Machold, R., Saunders, A., Levandowski, K., Zaniewski, H., Schuman, B., et al. (2020). Innovations present in the primate interneuron repertoire. Nature *586*, 262-269. 10.1038/s41586-020-2781-z.
26. Beaulieu-Laroche, L., Brown, N.J., Hansen, M., Toloza, E.H.S., Sharma, J., Williams, Z.M., Frosch, M.P., Cosgrove, G.R., Cash, S.S., and Harnett, M.T. (2021). Allometric rules for mammalian cortical layer 5 neuron biophysics. Nature *600*, 274-278. 10.1038/s41586-021-04072-3.
27. Caglayan, E., Ayhan, F., Liu, Y., Vollmer, R.M., Oh, E., Sherwood, C.C., Preuss, T.M., Yi, S.V., and Konopka, G. (2023). Molecular features driving cellular complexity of human brain evolution. Nature *620*, 145-153. 10.1038/s41586-023-06338-4.
28. Micali, N., Ma, S., Li, M., Kim, S.K., Mato-Blanco, X., Sindhu, S.K., Arellano, J.I., Gao, T., Shibata, M., Gobeske, K.T., et al. (2023). Molecular programs of regional specification and neural stem cell fate progression in macaque telencephalon. Science *382*, eadf3786. 10.1126/science.adf3786.
29. Rash, B.G., Duque, A., Morozov, Y.M., Arellano, J.I., Micali, N., and Rakic, P. (2019). Gliogenesis in the outer subventricular zone promotes enlargement and gyrification of the primate cerebrum. Proceedings of the National Academy of Sciences of the United States of America *116*, 7089-7094. 10.1073/pnas.1822169116.
30. Luria, V., Ma, S., Shibata, M., Pattabiraman, K., and Sestan, N. (2023). Molecular and cellular mechanisms of human cortical connectivity. Curr Opin Neurobiol *80*, 102699. 10.1016/j.conb.2023.102699.
31. Li, M., Santpere, G., Imamura Kawasawa, Y., Evgrafov, O.V., Gulden, F.O., Pochareddy, S., Sunkin, S.M., Li, Z., Shin, Y., Zhu, Y., et al. (2018). Integrative functional genomic analysis of human brain development and neuropsychiatric risks. Science *362*. 10.1126/science.aat7615.
32. Erdogan, F., Ullmann, R., Chen, W., Schubert, M., Adolph, S., Hultschig, C., Kalscheuer, V., Ropers, H.H., Spaich, C., and Tzschach, A. (2007). Characterization of a 5.3 Mb deletion in 15q14 by comparative genomic hybridization using a whole genome "tiling

path" BAC array in a girl with heart defect, cleft palate, and developmental delay. Am J Med Genet A *143A*, 172-178. 10.1002/ajmg.a.31541.

33. Jin, T., Rehani, P., Ying, M., Huang, J., Liu, S., Roussos, P., and Wang, D. (2021). scGRNom: a computational pipeline of integrative multi-omics analyses for predicting cell-type disease genes and regulatory networks. Genome Med *13*, 95. 10.1186/s13073-021-00908-9.
34. Dupacova, N., Antosova, B., Paces, J., and Kozmik, Z. (2021). Meis homeobox genes control progenitor competence in the retina. Proceedings of the National Academy of Sciences of the United States of America *118*. 10.1073/pnas.2013136118.
35. Negishi, Y., Miya, F., Hattori, A., Mizuno, K., Hori, I., Ando, N., Okamoto, N., Kato, M., Tsunoda, T., Yamasaki, M., et al. (2015). Truncating mutation in NFIA causes brain malformation and urinary tract defects. Hum Genome Var *2*, 15007. 10.1038/hgv.2015.7.
36. Cadwell, C.R., Palasantza, A., Jiang, X., Berens, P., Deng, Q., Yilmaz, M., Reimer, J., Shen, S., Bethge, M., Tolias, K.F., et al. (2016). Electrophysiological, transcriptomic and morphologic profiling of single neurons using Patch-seq. Nat Biotechnol *34*, 199-203. 10.1038/nbt.3445.
37. Bos, J.L. (2003). Epac: a new cAMP target and new avenues in cAMP research. Nat Rev Mol Cell Biol *4*, 733-738. 10.1038/nrm1197.
38. de Rooij, J., Zwartkruis, F.J., Verheijen, M.H., Cool, R.H., Nijman, S.M., Wittinghofer, A., and Bos, J.L. (1998). Epac is a Rap1 guanine-nucleotide-exchange factor directly activated by cyclic AMP. Nature *396*, 474-477. 10.1038/24884.
39. Woolfrey, K.M., Srivastava, D.P., Photowala, H., Yamashita, M., Barbolina, M.V., Cahill, M.E., Xie, Z., Jones, K.A., Quilliam, L.A., Prakriya, M., and Penzes, P. (2009). Epac2 induces synapse remodeling and depression and its disease-associated forms alter spines. Nature neuroscience *12*, 1275-1284. 10.1038/nn.2386.
40. Consortium, G.T. (2015). Human genomics. The Genotype-Tissue Expression (GTEx) pilot analysis: multitissue gene regulation in humans. Science *348*, 648-660. 10.1126/science.1262110.
41. Satterstrom, F.K., Kosmicki, J.A., Wang, J., Breen, M.S., De Rubeis, S., An, J.Y., Peng, M., Collins, R., Grove, J., Klei, L., et al. (2020). Large-Scale Exome Sequencing Study Implicates Both Developmental and Functional Changes in the Neurobiology of Autism. Cell *180*, 568-584 e523. 10.1016/j.cell.2019.12.036.
42. Katayama, Y., Nishiyama, M., Shoji, H., Ohkawa, Y., Kawamura, A., Sato, T., Suyama, M., Takumi, T., Miyakawa, T., and Nakayama, K.I. (2016). CHD8 haploinsufficiency results in autistic-like phenotypes in mice. Nature *537*, 675-679. 10.1038/nature19357.
43. Bernier, R., Golzio, C., Xiong, B., Stessman, H.A., Coe, B.P., Penn, O., Witherspoon, K., Gerdts, J., Baker, C., Vulto-van Silfhout, A.T., et al. (2014). Disruptive CHD8 mutations define a subtype of autism early in development. Cell *158*, 263-276. 10.1016/j.cell.2014.06.017.
44. Durak, O., Gao, F., Kaeser-Woo, Y.J., Rueda, R., Martorell, A.J., Nott, A., Liu, C.Y., Watson, L.A., and Tsai, L.H. (2016). Chd8 mediates cortical neurogenesis via transcriptional regulation of cell cycle and Wnt signaling. Nature neuroscience *19*, 1477-1488. 10.1038/nn.4400.
45. Kepecs, A., and Fishell, G. (2014). Interneuron cell types are fit to function. Nature *505*, 318-326. 10.1038/nature12983.

46. Jones, K.A., Sumiya, M., Woolfrey, K.M., Srivastava, D.P., and Penzes, P. (2019). Loss of EPAC2 alters dendritic spine morphology and inhibitory synapse density. Molecular and cellular neurosciences *98*, 19-31. 10.1016/j.mcn.2019.05.001.
47. Berry-Kravis, E., Hicar, M., and Ciurlionis, R. (1995). Reduced cyclic AMP production in fragile X syndrome: cytogenetic and molecular correlations. Pediatr Res *38*, 638-643. 10.1203/00006450-199511000-00002.
48. Berry-Kravis, E.M., Harnett, M.D., Reines, S.A., Reese, M.A., Ethridge, L.E., Outterson, A.H., Michalak, C., Furman, J., and Gurney, M.E. (2021). Inhibition of phosphodiesterase-4D in adults with fragile X syndrome: a randomized, placebo-controlled, phase 2 clinical trial. Nat Med *27*, 862-870. 10.1038/s41591-021-01321-w.
49. Sherwood, C.C., Subiaul, F., and Zawidzki, T.W. (2008). A natural history of the human mind: tracing evolutionary changes in brain and cognition. Journal of anatomy *212*, 426-454. 10.1111/j.1469-7580.2008.00868.x.
50. Wang, L., Pang, K., Zhou, L., Cebrian-Silla, A., Gonzalez-Granero, S., Wang, S., Bi, Q., White, M.L., Ho, B., Li, J., et al. (2023). A cross-species proteomic map reveals neoteny of human synapse development. Nature *622*, 112-119. 10.1038/s41586-023-06542-2.
51. Hao, Y., Hao, S., Andersen-Nissen, E., Mauck, W.M., 3rd, Zheng, S., Butler, A., Lee, M.J., Wilk, A.J., Darby, C., Zager, M., et al. (2021). Integrated analysis of multimodal single-cell data. Cell *184*, 3573-3587 e3529. 10.1016/j.cell.2021.04.048.
52. Stuart, T., Srivastava, A., Madad, S., Lareau, C.A., and Satija, R. (2021). Single-cell chromatin state analysis with Signac. Nat Methods *18*, 1333-1341. 10.1038/s41592-021-01282-5.
53. Schep, A.N., Wu, B., Buenrostro, J.D., and Greenleaf, W.J. (2017). chromVAR: inferring transcription-factor-associated accessibility from single-cell epigenomic data. Nat Methods *14*, 975-978. 10.1038/nmeth.4401.
54. Hahne, F., and Ivanek, R. (2016). Visualizing Genomic Data Using Gviz and Bioconductor. Methods Mol Biol *1418*, 335-351. 10.1007/978-1-4939-3578-9_16.
55. Fornes, O., Castro-Mondragon, J.A., Khan, A., van der Lee, R., Zhang, X., Richmond, P.A., Modi, B.P., Correard, S., Gheorghe, M., Baranasic, D., et al. (2020). JASPAR 2020: update of the open-access database of transcription factor binding profiles. Nucleic Acids Res *48*, D87-D92. 10.1093/nar/gkz1001.
56. Cao, J., Spielmann, M., Qiu, X., Huang, X., Ibrahim, D.M., Hill, A.J., Zhang, F., Mundlos, S., Christiansen, L., Steemers, F.J., et al. (2019). The single-cell transcriptional landscape of mammalian organogenesis. Nature *566*, 496-502. 10.1038/s41586-019-0969-x.
57. Amezquita, R.A., Lun, A.T.L., Becht, E., Carey, V.J., Carpp, L.N., Geistlinger, L., Marini, F., Rue-Albrecht, K., Risso, D., Soneson, C., et al. (2020). Orchestrating single-cell analysis with Bioconductor. Nat Methods *17*, 137-145. 10.1038/s41592-019-0654-x.
58. Korsunsky, I., Millard, N., Fan, J., Slowikowski, K., Zhang, F., Wei, K., Baglaenko, Y., Brenner, M., Loh, P.R., and Raychaudhuri, S. (2019). Fast, sensitive and accurate integration of single-cell data with Harmony. Nat Methods *16*, 1289-1296. 10.1038/s41592-019-0619-0.
59. Durinck, S., Spellman, P.T., Birney, E., and Huber, W. (2009). Mapping identifiers for the integration of genomic datasets with the R/Bioconductor package biomaRt. Nat Protoc *4*, 1184-1191. 10.1038/nprot.2009.97.

60. Qiu, X., Mao, Q., Tang, Y., Wang, L., Chawla, R., Pliner, H.A., and Trapnell, C. (2017). Reversed graph embedding resolves complex single-cell trajectories. Nat Methods *14*, 979-982. 10.1038/nmeth.4402.
61. Lawrence, M., Huber, W., Pages, H., Aboyoun, P., Carlson, M., Gentleman, R., Morgan, M.T., and Carey, V.J. (2013). Software for computing and annotating genomic ranges. PLoS Comput Biol *9*, e1003118. 10.1371/journal.pcbi.1003118.
62. Huber, W., Carey, V.J., Gentleman, R., Anders, S., Carlson, M., Carvalho, B.S., Bravo, H.C., Davis, S., Gatto, L., Girke, T., et al. (2015). Orchestrating high-throughput genomic analysis with Bioconductor. Nat Methods *12*, 115-121. 10.1038/nmeth.3252.
63. Gu, Z., Eils, R., and Schlesner, M. (2016). Complex heatmaps reveal patterns and correlations in multidimensional genomic data. Bioinformatics *32*, 2847-2849. 10.1093/bioinformatics/btw313.
64. Rainer, J., Gatto, L., and Weichenberger, C.X. (2019). ensembldb: an R package to create and use Ensembl-based annotation resources. Bioinformatics *35*, 3151-3153. 10.1093/bioinformatics/btz031.
65. Leng, N., Dawson, J.A., Thomson, J.A., Ruotti, V., Rissman, A.I., Smits, B.M., Haag, J.D., Gould, M.N., Stewart, R.M., and Kendziorski, C. (2013). EBSeq: an empirical Bayes hierarchical model for inference in RNA-seq experiments. Bioinformatics *29*, 1035-1043. 10.1093/bioinformatics/btt087.
66. Zhou, Y., Zhou, B., Pache, L., Chang, M., Khodabakhshi, A.H., Tanaseichuk, O., Benner, C., and Chanda, S.K. (2019). Metascape provides a biologist-oriented resource for the analysis of systems-level datasets. Nat Commun *10*, 1523. 10.1038/s41467-019-09234-6.
67. Zhang, Y., Liu, T., Meyer, C.A., Eeckhoute, J., Johnson, D.S., Bernstein, B.E., Nusbaum, C., Myers, R.M., Brown, M., Li, W., and Liu, X.S. (2008). Model-based analysis of ChIP-Seq (MACS). Genome Biol *9*, R137. 10.1186/gb-2008-9-9-r137.
68. Onorati, M., Li, Z., Liu, F., Sousa, A.M.M., Nakagawa, N., Li, M., Dell'Anno, M.T., Gulden, F.O., Pochareddy, S., Tebbenkamp, A.T.N., et al. (2016). Zika Virus Disrupts Phospho-TBK1 Localization and Mitosis in Human Neuroepithelial Stem Cells and Radial Glia. Cell Rep *16*, 2576-2592. 10.1016/j.celrep.2016.08.038.
69. Shen, M., Sirois, C.L., Guo, Y., Li, M., Dong, Q., Mendez-Albelo, N.M., Gao, Y., Khullar, S., Kissel, L., Sandoval, S.O., et al. (2023). Species-specific FMRP regulation of RACK1 is critical for prenatal cortical development. Neuron. 10.1016/j.neuron.2023.09.014.
70. Stuart, T., Butler, A., Hoffman, P., Hafemeister, C., Papalexi, E., Mauck, W.M., 3rd, Hao, Y., Stoeckius, M., Smibert, P., and Satija, R. (2019). Comprehensive Integration of Single-Cell Data. Cell *177*, 1888-1902 e1821. 10.1016/j.cell.2019.05.031.
71. Stuart, T., Srivastava, A., Madad, S., Lareau, C.A., and Satija, R. (2022). Author Correction: Single-cell chromatin state analysis with Signac. Nat Methods *19*, 257. 10.1038/s41592-022-01393-7.
72. Young, M.D., and Behjati, S. (2020). SoupX removes ambient RNA contamination from droplet-based single-cell RNA sequencing data. Gigascience *9*. 10.1093/gigascience/giaa151.
73. McGinnis, C.S., Murrow, L.M., and Gartner, Z.J. (2019). DoubletFinder: Doublet Detection in Single-Cell RNA Sequencing Data Using Artificial Nearest Neighbors. Cell Syst *8*, 329-337 e324. 10.1016/j.cels.2019.03.003.

832 74. Butler, A., Hoffman, P., Smibert, P., Papalexi, E., and Satija, R. (2018). Integrating single-
833 cell transcriptomic data across different conditions, technologies, and species. Nat
834 Biotechnol *36*, 411-420. 10.1038/nbt.4096.
835 75. Becht, E., McInnes, L., Healy, J., Dutertre, C.A., Kwok, I.W.H., Ng, L.G., Ginhoux, F.,
836 and Newell, E.W. (2018). Dimensionality reduction for visualizing single-cell data using
837 UMAP. Nat Biotechnol. 10.1038/nbt.4314.
838 76. Haghverdi, L., Lun, A.T.L., Morgan, M.D., and Marioni, J.C. (2018). Batch effects in
839 single-cell RNA-sequencing data are corrected by matching mutual nearest neighbors. Nat
840 Biotechnol *36*, 421-427. 10.1038/nbt.4091.
841 77. Dong, Q., Kim, J., Nguyen, L., Bu, Q., and Chang, Q. (2020). An Astrocytic Influence on
842 Impaired Tonic Inhibition in Hippocampal CA1 Pyramidal Neurons in a Mouse Model of
843 Rett Syndrome. J Neurosci *40*, 6250-6261. 10.1523/JNEUROSCI.3042-19.2020.
844 78. Hagemann-Jensen, M., Ziegenhain, C., Chen, P., Ramskold, D., Hendriks, G.J., Larsson,
845 A.J.M., Faridani, O.R., and Sandberg, R. (2020). Single-cell RNA counting at allele and
846 isoform resolution using Smart-seq3. Nat Biotechnol *38*, 708-714. 10.1038/s41587-020-
847 0497-0.
848 79. Dobin, A., Davis, C.A., Schlesinger, F., Drenkow, J., Zaleski, C., Jha, S., Batut, P.,
849 Chaisson, M., and Gingeras, T.R. (2013). STAR: ultrafast universal RNA-seq aligner.
850 Bioinformatics *29*, 15-21. 10.1093/bioinformatics/bts635.
851 80. Gao, Y., Shen, M., Gonzalez, J.C., Dong, Q., Kannan, S., Hoang, J.T., Eisinger, B.E.,
852 Pandey, J., Javadi, S., Chang, Q., et al. (2020). RGS6 Mediates Effects of Voluntary
853 Running on Adult Hippocampal Neurogenesis. Cell Rep *32*, 107997.
854 10.1016/j.celrep.2020.107997.
855 81. Livak, K.J., and Schmittgen, T.D. (2001). Analysis of relative gene expression data using
856 real-time quantitative PCR and the 2(-Delta Delta C(T)) Method. Methods *25*, 402-408.
857 10.1006/meth.2001.1262.
858 82. Gao, Y., Su, J., Guo, W., Polich, E.D., Magyar, D.P., Xing, Y., Li, H., Smrt, R.D., Chang,
859 Q., and Zhao, X. (2015). Inhibition of miR-15a Promotes BDNF Expression and Rescues
860 Dendritic Maturation Deficits in MeCP2-Deficient Neurons. Stem Cells *33*, 1618-1629.
861 10.1002/stem.1950.
862 83. Guo, Y., Shen, M., Dong, Q., Mendez-Albelo, N.M., Huang, S.X., Sirois, C.L., Le, J., Li,
863 M., Jarzembowski, E.D., Schoeller, K.A., et al. (2023). Elevated levels of FMRP-target
864 MAP1B impair human and mouse neuronal development and mouse social behaviors via
865 autophagy pathway. Nat Commun *14*, 3801. 10.1038/s41467-023-39337-0.
866
867